

Raman spectroscopy characterization of TiO₂ rutile nanocrystals

T. Mazza, E. Barborini,* P. Piseri, and P. Milani†

CIMAINA, and Dipartimento di Fisica, Università di Milano, via Celoria 16, I-20133 Milano, Italy

D. Cattaneo, A. Li Bassi, and C. E. Bottani

NEMAS, CNISM and Dipartimento di Ingegneria Nucleare, Politecnico di Milano, Via Ponzio 34/3 I-20133 Milano, Italy

C. Ducati

Department of Material Science and Metallurgy, University of Cambridge, Cambridge, CB2 3QZ, United Kingdom

(Received 7 August 2006; revised manuscript received 1 November 2006; published 11 January 2007)

We report the characterization by Raman spectroscopy of rutile nanocrystals embedded in cluster-assembled TiO₂ films produced by supersonic cluster beam deposition. Thermal annealing of the as-deposited films promotes the growth of rutile and anatase nanoparticles with a dimension distribution peaked around 10 nm. We show that a phonon confinement model is not adequate to explain the features of the lattice dynamics of rutile nanocrystals. The coexistence of the two crystalline phases allows us to identify the role of chemical and structural inhomogeneities in the film potentially affecting the Raman spectra. Our results suggest that the lattice dynamics of rutile nanocrystals is influenced by the dielectric constant of the cluster-assembled films.

DOI: [10.1103/PhysRevB.75.045416](https://doi.org/10.1103/PhysRevB.75.045416)

PACS number(s): 61.46.-w, 78.30.-j, 63.22.+m, 68.55.-a

I. INTRODUCTION

Transition metal oxide nanocrystals hold great potential for a variety of functional and structural applications including chemical sensing,^{1,2} catalysis,^{3,4} and nanomedicine;⁵ this has stimulated a considerable experimental and theoretical effort in order to understand how the dimensions, crystalline phase, and stoichiometry of nanoparticles affect their physico-chemical properties. Size effects in ionic nanocrystals are intimately related to a departure from bulk lattice parameters (lattice expansion or contraction) and to a modification of lattice dynamics.⁶⁻⁸ These features have been related to the presence of chemical complexes at the surface^{7,9} and/or a variation of the ionicity of the bonding,^{6,7} however, a fundamental understanding is still lacking.

The lattice dynamics modifications in oxide nanoparticles can be explained by considering that translational invariance is significantly broken when the crystal extension is in the 1–100 nm range and a description of atomic vibrations in such a domain in terms of phonons with a well-defined wave vector is no longer valid. This is the basis of the so-called phonon confinement model (PCM) developed to describe the intensity of the first-order Raman scattering from semiconductor nanocrystals.^{10,11} In PCM, a phenomenological confinement function is used to fit the Raman spectrum of an assembly of nanoparticles with a known size distribution. The interpretation of the size dependence of Raman spectra is thus of both fundamental and practical interest for the understanding of lattice dynamics in oxide nanoparticles and as a method for rapid characterization of size distribution in polydisperse assemblies of nanoparticles.^{12,13}

Among ionic systems, nanostructured titanium dioxide (ns-TiO₂) is one of the most studied: a conspicuous amount of data are reported in literature showing that the optical, electronic, and vibrational properties become size dependent for TiO₂ particles smaller than few tens of nanometers.¹³⁻¹⁵ Titanium dioxide exists in nature in three major crystalline

structures: rutile, anatase, and brookite,¹⁶⁻¹⁸ only rutile and anatase have properties of interest for applications so that they have been extensively characterized.¹⁶⁻¹⁸ Rutile is thermodynamically stable and it can be obtained by thermal annealing of amorphous titania which transforms into anatase at moderate temperatures; in the bulk the transition to rutile takes place around 800–1000 °C.

Nanostructured TiO₂ can be produced by sol-gel, hydrolysis, chemical, and physical vapor deposition.^{8,13,16-20} In order to study the factors influencing different properties, phase stabilities, and size-dependent structural phase transitions it is necessary to produce samples characterized by a single crystalline phase and a well-defined stoichiometry and surface chemistry. This represents a major challenge for many of the synthetic methods reported above since the coexistence of different phases, the presence of defects and/or adsorbates is practically unavoidable, making the comparison between results obtained on systems nominally similar, but produced with different synthetic methods, highly questionable.^{8,19}

Anatase ns-TiO₂ has been extensively characterized by Raman scattering: the modification of the Raman spectral features due to size effects have been variously interpreted as originating from phonon confinement^{7,14} or nonstoichiometry.^{20,21} The majority of the published studies refer to phonon confinement as the main mechanism responsible for the observed size-dependent Raman features,⁷ however, recently limitations of PCM have been pointed out.¹⁹

Quite surprisingly, no systematic characterization of the lattice dynamics of rutile nanocrystals is available so far, despite the fact that this tetragonal form of TiO₂ has dielectric, optical, and elastic properties of considerable interest.²² Pressure and temperature dependence of the static dielectric constants and Raman spectra of bulk rutile are available in literature,²² and for the nanocrystalline counterpart the evidence of linear lattice expansion has been recently reported.⁶

The lack of systematic Raman characterization of size effects in rutile nanocrystals is probably due to the difficulty of

producing rutile nanoparticles with a controlled stoichiometry, mass distribution and without contaminations.⁸ Parker and Siegel have characterized by Raman spectroscopy nanostructured titania films produced by gas-phase aggregation methods in understoichiometric conditions where anatase and rutile phases coexist.²⁰ Modifications of the Raman spectra of rutile and anatase have been attributed to nonstoichiometry of the samples.

Recently we have demonstrated that it is possible to produce nanocrystalline TiO₂ thin films with independently controlled crystal size and anatase/rutile ratio.²³ Here we present a Raman characterization of the rutile component of the nanocrystalline film showing the failure of the PCM to explain the observed modifications in the spectra due to the reduced dimensions of the rutile crystals.

II. EXPERIMENT

We have produced nanostructured TiO₂ films by deposition of a supersonic beam of clusters generated by a pulsed microplasma cluster source (PMCS).^{24,25} The principle of operation of a PMCS has been described in detail elsewhere,^{24,25} here we briefly describe the elements relevant for the system under study. The formation of clusters is initiated by the injection of a helium pulse towards a titanium target rod placed in the PMCS reaction chamber. A pulsed electric discharge ionizes the gas forming an aerodynamically confined plasma that erodes the target.²⁵ Thermalization and condensation of the sputtered Ti atoms takes place in an oxygen-deficient atmosphere favoring the formation of substoichiometric rutile and anatase clusters.²³ The cluster-helium mixture then expands through a nozzle in a high vacuum region generating a supersonic beam which is intercepted by a substrate where a nanostructured film is grown. The kinetic energy of the clusters is such that fragmentation upon landing is negligible and the film growth takes place in a ballistic regime²⁶ at a rate of roughly 10 nm/min.

Substoichiometric oxidation of free clusters is confirmed by time of flight mass spectrometry and by *in situ* near-edge x-ray absorption fine structure (NEXAFS) spectroscopy.²⁷ Air exposure and subsequent thermal annealing at mild conditions promote the oxidation of the films due to their high porosity.

The films have been deposited on silicon and alumina substrates and annealed at 450 °C for 4 hours in air. They have subsequently been characterized by micro-Raman spectroscopy using a triple grating Jobin-Yvon T64000 spectrometer with the 514.5 nm line of an argon ion laser. Structural characterizations have been performed by a transmission electron microscope (TEM) JEOL JEM-4000EX, 400 kV.

III. RESULTS AND DISCUSSION

Figure 1(a) shows the typical nanocrystalline structure of a cluster-assembled film annealed as described in the experimental section. An analysis of the lattice spacing demonstrates the coexistence of anatase and rutile nanoparticles. This particular film nanostructure can be obtained by depositing anatase and rutile clusters embedded in an amorphous

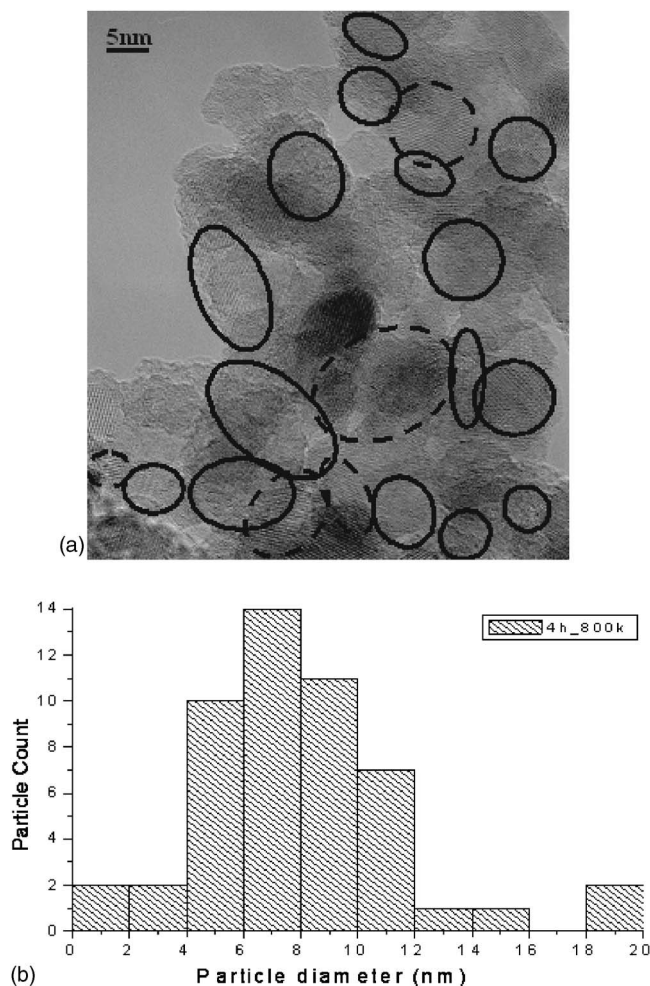


FIG. 1. (a) TEM micrograph of a cluster-assembled TiO₂ film annealed for 4 h at 450 °C. Continuous and dotted circles identify anatase and rutile nanocrystalline regions respectively. (b) Anatase and rutile particle size distribution in the annealed films.

matrix,²³ the subsequent thermal annealing in air causes, in the deposited material, both crystal growth and nucleation of different seeds. The nucleation or growth of rutile and anatase are characterized by different activation energies:⁹ when rutile nuclei are present, the growth of this phase is kinetically favored whereas the nucleation and growth of anatase nanocrystals takes place where rutile nuclei are absent.²³ A mild temperature annealing causes the evolution towards a well-defined crystal structure without inducing a direct phase transition from anatase to rutile.

In Fig. 1(b) we report the typical size distribution of the nanocrystals forming the films: it is peaked below 10 nm both for anatase and rutile nanoparticles, even for relatively high annealing temperatures,^{26,28,29} as confirmed by a systematic analysis of the TEM micrographs taken from several films used for the Raman characterization (see below). This analysis shows that we produced films where rutile and anatase nanocrystals with the same size distribution are uniformly distributed.

A typical Raman spectrum of a cluster-assembled film is reported in Fig. 2 where the E_g (144 cm⁻¹) anatase mode and the E_g (447 cm⁻¹) and A_{1g} (612 cm⁻¹) rutile modes can be

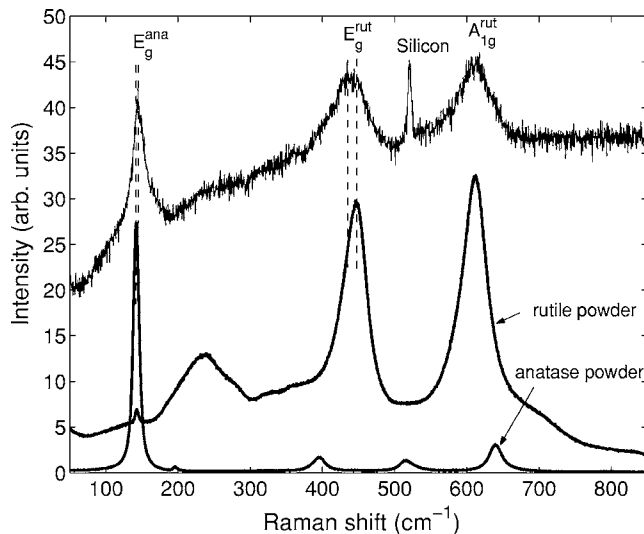


FIG. 2. Raman spectrum of a cluster-assembled film deposited on silicon and annealed at 450 °C for 4 h. Anatase and rutile spectral features are present. The E_g anatase mode has an average peak position of 145.5 cm^{-1} (standard deviation: 0.9 cm^{-1}); the E_g rutile mode has an average peak position of 440.4 cm^{-1} (standard deviation: 2.5 cm^{-1}); the A_g rutile mode has an average peak position of 611.8 cm^{-1} (standard deviation: 1.4 cm^{-1}). Raman spectra of commercially available rutile and anatase microcrystalline samples are reported for comparison.

recognized.¹⁹ A sharp bulk silicon peak coming from the substrate of the film is visible at 521 cm^{-1} . The E_g anatase mode shows a blue shift and an asymmetric broadening which can be related to the variation of the dimensions of the nanoparticles, the variation of the spectral features of this mode have been reported in the literature for a wide variety of nanostructured TiO_2 systems and fitted with PCM.^{8,13,19} As anticipated in the Introduction, the Raman features of the rutile phase are far less characterized: a red shift attributed to nonstoichiometric effects has been reported for the E_g rutile mode.²⁰

We characterized twenty films by taking several spectra at random positions on each film in order to map the size-dependent modification of the Raman peaks both for the anatase and rutile nanocrystals. Since the two phases are coexisting and uniformly distributed in the films, we can follow at the same time the influence of the inhomogeneities in the particle size distribution, stoichiometry, matrix density etc., on the lattice dynamics.

We have analyzed the Raman spectra by Lorentzian and Gaussian multiplex fitting. The results show some general trends in the behavior of the peaks' positions: the anatase E_g mode shows a blue shift (maximum shift of 3 cm^{-1}), the rutile E_g mode shows a red shift (maximum shift of 10.7 cm^{-1}), and the rutile A_g mode a random shift (maximum shift of 4.2 cm^{-1}).

At the nanoscale, the presence of oxygen vacancies can substantially affect the physical and chemical properties of titania.¹⁸ The evaluation of the role of stoichiometry is problematic, in particular in nanostructured systems, due to the extreme difficulty in determining quantitatively the $[\text{O}]/[\text{Ti}]$ ratio. For our samples, the thermal treatment reduces the pos-

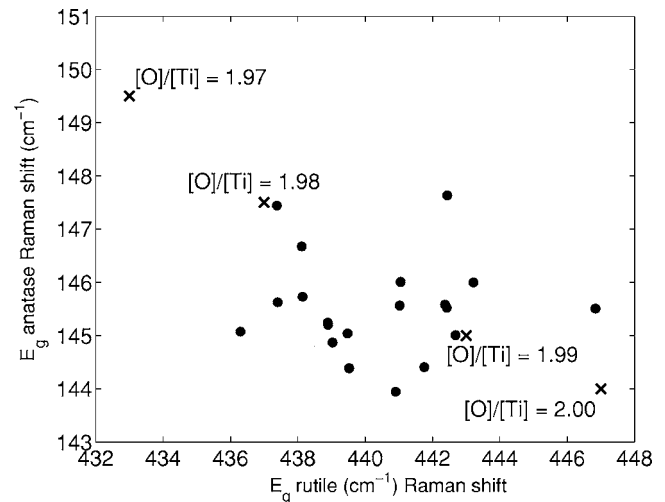


FIG. 3. Comparison between the expected correlation between the positions of the anatase and rutile E_g peaks (crosses) as taken from Ref. 20 and the correlation of the same peaks obtained from our data (circles). Data from literature are characterized by an uncertainty of 1 cm^{-1} both for the anatase phase (y axis) and for the rutile phase (x axis).

sibility of deviations from $[\text{O}]/[\text{Ti}]=2$, however we cannot exclude that stoichiometric inhomogeneities can be present especially at small scales. In any case we can assume that the annealing-induced oxidation, even if incomplete, is independent from the crystalline phase of the nanoparticles. Using the calibration curves of the Raman spectrum of nanophase TiO_2 obtained by Parker and Siegel,²⁰ we plot the correlation expected between the E_g anatase peak and the E_g rutile peak at the variation of the $[\text{O}]/[\text{Ti}]$ ratio and we compare it with the correlation obtained from the Raman peak of our samples (Fig. 3). One can easily recognize that our data do not follow the trend expected for stoichiometry variation and we can conclude that observed shifts in Raman peaks, and hence the lattice dynamics of the rutile and anatase nanocrystals, are not affected by nonstoichiometric effects.

In order to check the validity of the PCM to describe the rutile vibrational spectra in confined systems, we used the standard approach assuming the breakdown of the phonon momentum selection rule $q \approx 0$ in nanocrystals.¹¹ The weight of the off-center phonons depends on a confinement function, and it increases as the crystallite size decreases; the phonon dispersion causes an asymmetric broadening and a shift of the Raman lines, which for spherical monodisperse nanocrystals and first-order scattering are described by

$$I(\omega) = \int_{BZ} \frac{|C(\vec{q})|^2}{[\omega - \omega(\vec{q})]^2 + \Gamma_0^2/2}, \quad (1)$$

$$|C(\vec{q})|^2 = \exp\left(-\frac{q^2 d^2}{16\pi^2}\right), \quad (2)$$

where Γ_0 is the Raman bulk linewidth, d is the crystallite size, and $\omega(q)$ is the \vec{q} -dependent phonon frequency. The confinement function reported in Eq. (2) accounts for a strong confinement of the phonons in the nanocrystal.¹¹ We

TABLE I. Parameters used in Eq. (1) for E_g and A_{1g} rutile modes calculation as shown in Fig. 4. The dispersion relations are obtained by interpolating data from Ref. 30. Γ_0 is full width at half maximum from reference spectra shown in Fig. 2. $\xi=cq/2\pi$ for the E_g mode, and $\xi=aq/2\pi$ for the A_{1g} mode, where $c=2.95$ Å and $a=4.59$ Å are, respectively, the lattice [001] and [110] constants for rutile structure.

Mode	E_g	A_{1g}
[001] dispersion relation	$\omega(q)_{001}=447+22[\cos(2\pi 1.43\xi)-1]\text{cm}^{-1}$	
[100] dispersion relation	$\omega(q)_{001}=447\text{ cm}^{-1}$	$\omega(q)_{001}=612\text{ cm}^{-1}$
[110] dispersion relation	$\omega(q)_{001}=447\text{ cm}^{-1}$	$\omega(q)_{001}=612-587.5\xi^2\text{ cm}^{-1}$
Γ_0	35 cm^{-1}	40 cm^{-1}

then calculated $I(\omega)$ [Eq. (1)] for the E_g and the A_{1g} rutile modes at various particle size values, using the data of Table I, obtained from powder reference samples and by interpolating neutron scattering data from Ref. 30. The calculations show that the effects of the phonon confinement become quite negligible within experimental error for rutile crystal sizes larger than 10 nm. This upper limit is of course somewhat arbitrary, since it depends on the choice of the confinement function.¹⁹ In Fig. 4 we report the correlation between the Raman shift and the peak width as calculated with the PCM for both the E_g and A_{1g} rutile peaks [Figs. 4(a) and 4(b)].

Figure 4(a) shows the comparison between the data calculated using the PCM and the experimental values obtained by characterizing different regions of the films and hence nanocrystals with different dimensions. The PCM is in reasonable agreement with the Raman results obtained for the rutile E_g mode, for which the Raman shifts and the widths correlation is reproduced by the model, although the TEM characterization of the samples does not support the expectation of such a wide range in mean particle size value. On the other hand, the behavior of the A_{1g} peak does not correspond at all with the prediction of the model [Fig. 4(b)] showing that the validity of the PCM seems to be limited to certain vibrational modes or crystalline symmetries.

Our experimental results can be discussed in the light of the theoretical description of the vibrational properties of nanometric AB_2 ionic clusters developed by Montanari *et al.*:³¹ this model shows the inadequacy of the PCM to describe the dependence of the lattice dynamics from the size of the particles. In particular, Montanari *et al.* have shown that the vibrational properties of the clusters depend on the dielectric constant of the medium in which they are embedded. In a nanoporous system such as the one we have produced with cluster beam deposition, an important influence on polarized modes comes from the local modulation of the density and therefore of the dielectric static constant of the medium embedding the nanocrystals. This is determined by the size and the packing of the deposited precursor clusters, annealing conditions, and film thickness.

In a bulk system, changes due to modulation in the surrounding dielectric constant are expected only for infrared (IR)-active modes, and the sensitivity to the dielectric properties of the medium is larger for the modes with the strongest IR activity. In a confined system, Raman-active modes are also slightly affected since in clusters the strict separation among IR active, Raman active, and silent modes is blurred;

frequency shifts are typically of the order of 0.5%, reaching up to 1% in the smallest clusters, and they are amplified when the large shift of IR active modes gives rise to level crossings.^{30,31} The rutile E_u IR-active mode (435 cm^{-1}), which is close to E_g Raman mode, could therefore become Raman active in nanosized particles. This could cause the

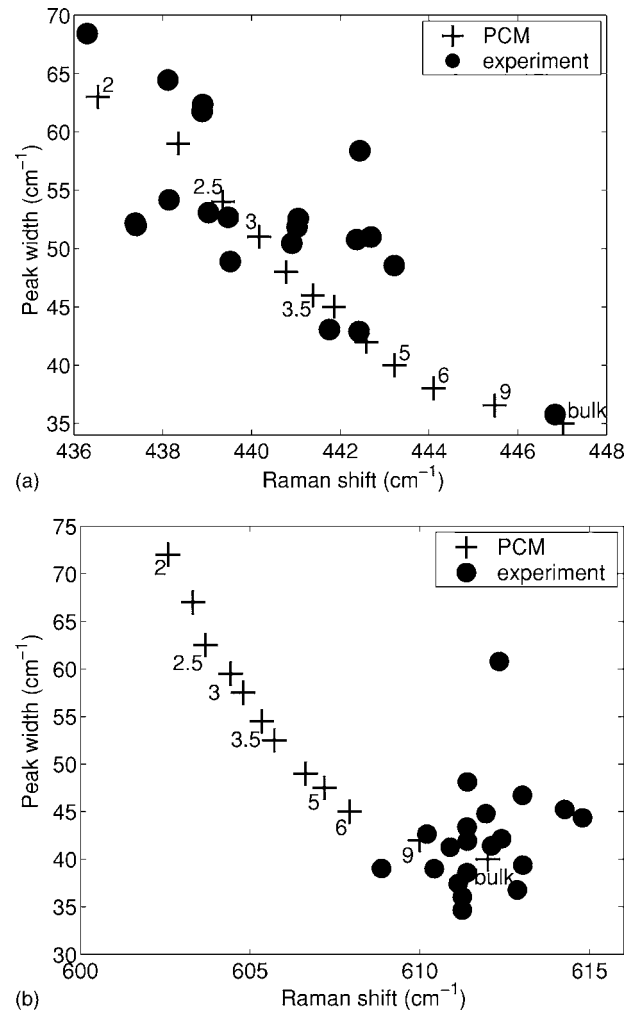


FIG. 4. (a) Comparison of the observed correlation of the Raman peak position and width of the E_g rutile peak (circles) with that calculated with the PCM model (plus signs). The numbers reported near the plus signs refer to the nanocrystal diameter used for the calculation with the PCM model. (b) Comparison of the observed correlation of the Raman peak position and width of the A_g rutile peak (circles) with that calculated with the PCM model (plus signs).

asymmetric shape of the E_g peak in the Raman spectra from our samples and its consequent red shift, determining therefore the different behavior of E_g and A_{1g} modes when the dimensions of the nanocrystals vary.

IV. SUMMARY

We have characterized by micro-Raman spectroscopy the lattice dynamics of rutile nanocrystals. By exploiting the possibility of growing films where anatase and rutile nanocrystals coexist and are uniformly distributed, we have separately studied different factors influencing the vibrational

spectra of the nanocrystalline TiO₂ tetragonal phase. Our results show the inadequacy of the phenomenological phonon confinement model to account for the size effects observed in rutile nanocrystals, suggesting the need of taking into account the influence of the environment (dielectric constant) where nanoparticles are embedded.³²

ACKNOWLEDGMENTS

We thank I.N. Kholmanov for his help in the preparation of the samples and P. Ballone for discussions. C.D. wishes to acknowledge the Royal Society for funding.

*Present address: Tethis srl, via Russoli 3, 20151 Milano, Italy.

†Corresponding author. Electronic address: pmilani@mi.infn.it

¹A. Kolmakov and M. Moskovits, *Annu. Rev. Mater. Res.* **34**, 151 (2004).

²See, for example, Special Issue *MRS Bull.* **24**(6) (1999).

³J. E. Spanier, R. D. Robinson, F. Zhang, S. W. Chan, and I. P. Herman, *Phys. Rev. B* **64**, 245407 (2001).

⁴S. Tsunekawa, K. Ishikawa, Z.-Q. Li, Y. Kawazoe, and A. Kasuya, *Phys. Rev. Lett.* **85**, 3440 (2000).

⁵R. Carbone, I. Marangi, A. Zanardi, L. Giorgetti, E. Chierici, G. Berlanda, A. Podestà, F. Fiorentini, G. Bongiorno, P. Piseri, P. G. Pelicci, and P. Milani, *Biomaterials* **27**, 3221 (2006).

⁶V. R. Palkar, P. Ayyub, S. Chattopadhyay, and M. Multani, *Phys. Rev. B* **53**, 2167 (1996).

⁷G. Li, J. Boerio-Gates, B. F. Woodfield, and L. Li, *Appl. Phys. Lett.* **85**, 2059 (2004).

⁸V. Swamy, A. Kutznetsov, L. S. Dubrovinsky, R. A. Caruso, D. G. Shchukin, and B. C. Muddle, *Phys. Rev. B* **71**, 184302 (2005).

⁹G. Li, L. Li, J. Boerio-Gates, and B. F. Woodfield, *J. Am. Chem. Soc.* **127**, 8659 (2005).

¹⁰H. Richter, Z. P. Wang, and L. Ley, *Solid State Commun.* **39**, 625 (1981).

¹¹I. H. Campbell and P. M. Fauchet, *Solid State Commun.* **58**, 739 (1986).

¹²C. E. Bottani, C. Mantini, P. Milani, M. Manfredini, A. Stella, P. Tognini, P. Cheyssac, and R. Kofman, *Appl. Phys. Lett.* **69**, 2409 (1996).

¹³D. Bersani, P. P. Lottici, and X.-Z. Ding, *Appl. Phys. Lett.* **72**, 73 (1998).

¹⁴A. Fujishima, T. N. Rao, and D. A. Tryk, *J. Photochem. Photobiol. C* **1**, 1 (2000).

¹⁵C. G. Granqvist, *Adv. Mater. (Weinheim, Ger.)* **15**, 1789 (2003).

¹⁶Shang-Di Mo and W. Y. Ching, *Phys. Rev. B* **51**, 13023 (1995).

¹⁷Zhongwu Wang, S. K. Saxena, V. Pishedda, H. P. Liermann, and C. S. Zha, *J. Phys.: Condens. Matter* **13**, 8317 (2001).

¹⁸U. Diebold, *Surf. Sci. Rep.* **48**, 53 (2003).

¹⁹A. Li Bassi, D. Cattaneo, V. Russo, C. E. Bottani, E. Barborini, T. Mazza, P. Piseri, P. Milani, F. O. Ernst, K. Wegner, and S. E. Pratsinis, *J. Appl. Phys.* **98**, 074305 (2005).

²⁰J. C. Parker and R. W. Siegel, *Appl. Phys. Lett.* **57**, 943 (1990).

²¹W. F. Zhang, Y. L. He, M. S. Zhang, Z. Yin, and Q. Chen, *J. Phys. D: Appl. Phys.* **33**, 912 (2000).

²²G. A. Samara and P. S. Peercy, *Phys. Rev. B* **7**, 1131 (1973).

²³T. Mazza, E. Barborini, I. N. Kholmanov, P. Piseri, G. Bongiorno, S. Vinati, P. Milani, C. Ducati, D. Cattaneo, A. Li Bassi, C. E. Bottani, A. M. Taurino, and P. Siciliano, *Appl. Phys. Lett.* **87**, 103108 (2005).

²⁴E. Barborini, P. Piseri, and P. Milani, *J. Phys. D: Appl. Phys.* **32**, L105 (1999).

²⁵H. Vahedi Tafreshi, P. Piseri, G. Benedek, and P. Milani, *J. Nanosci. Nanotechnol.* **6**, 1140 (2006).

²⁶I. N. Kholmanov, E. Barborini, S. Vinati, P. Piseri, A. Podestà, C. Ducati, C. Lenardi, and P. Milani, *Nanotechnology* **14**, 1168 (2003).

²⁷P. Piseri, T. Mazza, G. Bongiorno, C. Lenardi, L. Ravagnan, F. Della Foglia, F. DiFonzo, M. Coreno, M. DeSimone, K. C. Prince, and P. Milani, *New J. Phys.* **8**, 136 (2006).

²⁸E. Barborini, I. N. Kholmanov, P. Piseri, C. Ducati, C. E. Bottani, and P. Milani, *Appl. Phys. Lett.* **81**, 3052 (2002).

²⁹E. Barborini, I. N. Kholmanov, A. M. Conti, P. Piseri, S. Vinati, P. Milani, and C. Ducati, *Eur. Phys. J. D* **24**, 277 (2003).

³⁰J. G. Traylor, H. G. Smith, R. M. Nicklow, and M. K. Wilkinson, *Phys. Rev. B* **3**, 3457 (1971).

³¹B. Montanari, P. Ballone, T. Mazza, and P. Milani, *J. Phys.: Condens. Matter* **17**, 3787 (2005).

³²T. P. Martin and L. Genzel, *Phys. Rev. B* **8**, 1630 (1973).